# Supporting Information

# Self-Supported $NiCo_2O_4/Cu_xO$ Nanoforest with Electronically Modulated Interfaces as Efficient Electrocatalyst for Overall Water Splitting

Qi Ouyang[a], Zuotao Lei*[a], Qun Li[b], Mingyang Li[a] and Chunhui Yang*[a,]

a MIIT Key Laboratory of Critical Materials Technology for New Energy Conversion and Storage, School of Chemistry and Chemical Engineering, Harbin Institute of Technology, Harbin, 150001, People's Republic of China

b National Key Laboratory of Science and Technology on Advanced Composites in Special Environments, and Center for Composite Materials and Structures, Harbin Institute of Technology, Harbin 150080, China.

* Corresponding author: leizuotao@hit.edu.cn; yangchh@hit.edu.cn

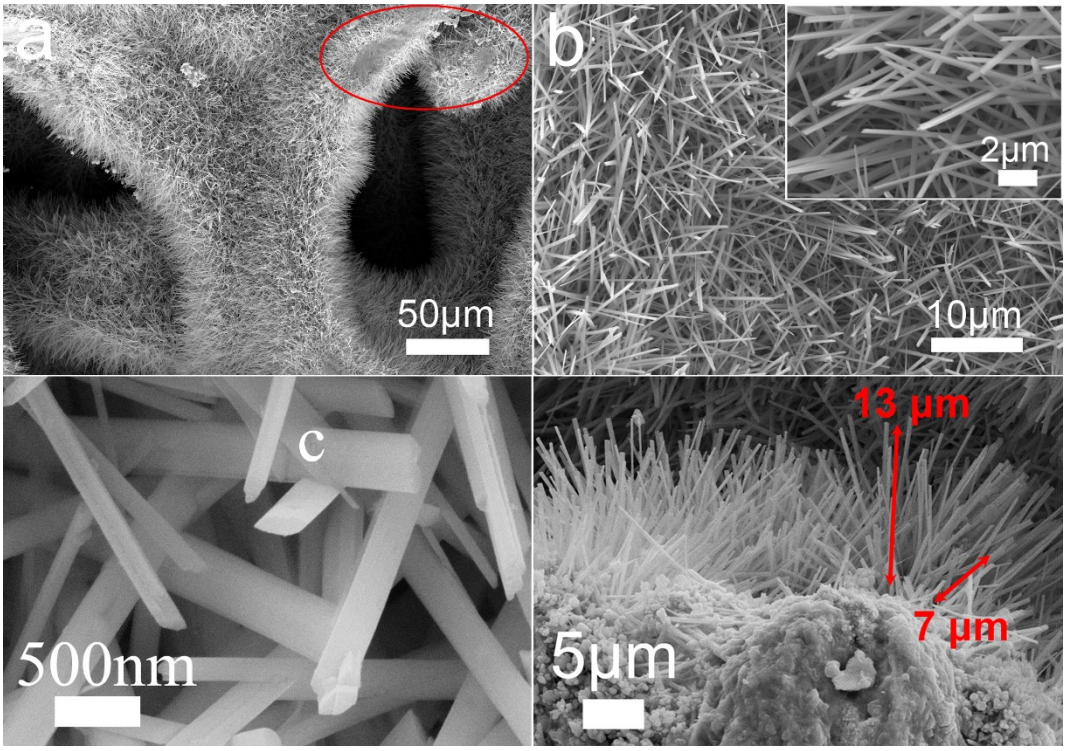


Fig. S1 (a-b) Low, (c) high magnification SEM images and (d) cross-section SEM image. of $Cu(OH)_2/Cu$. The region enclosed by the red circles is made by pressing $Cu(OH)_2/Cu$ on the conductive adhesive with tweezers.

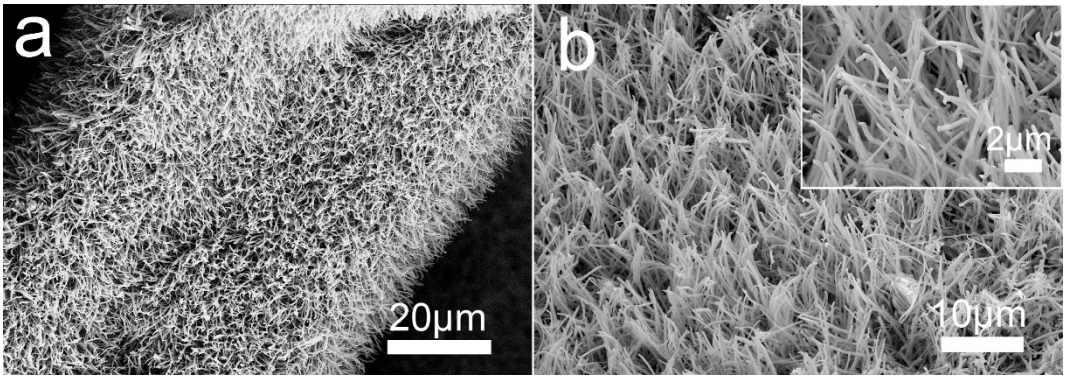


Fig. S2 (a) Low and (b) high magnification SEM images of $Cu_xO/Cu$.

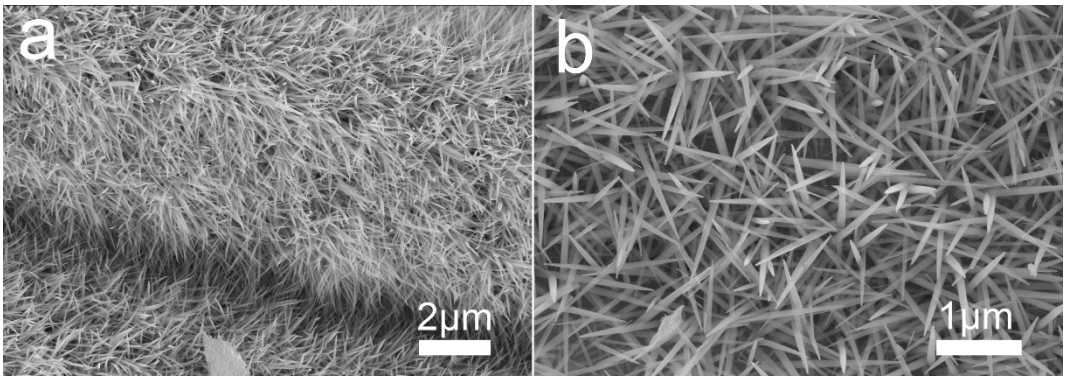


Fig. S3 (a) Low and (b) high magnification SEM images of NiCo-precursor/Cu.

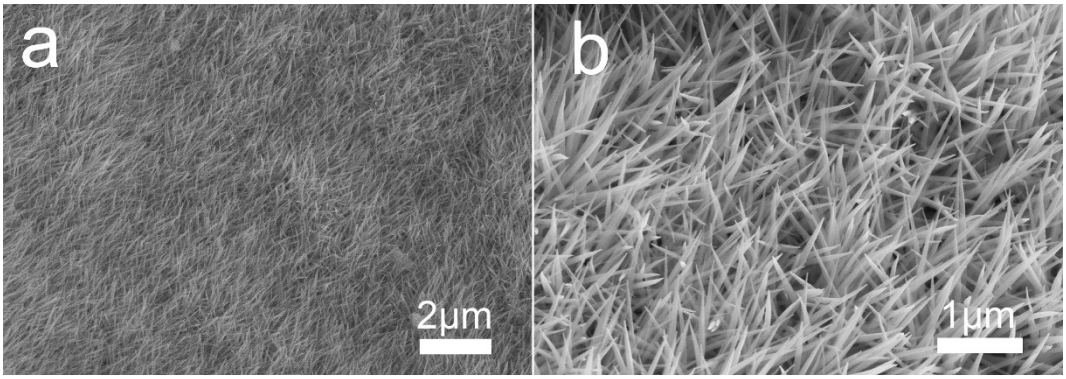


Fig. S4 (a) Low and (b) high magnification SEM images of $NiCo_2O_4$/Cu.

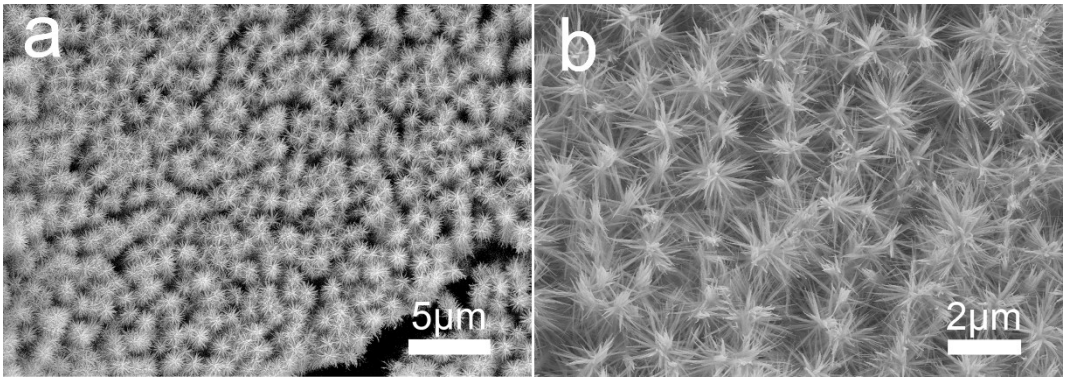


Fig. S5 (a) Low and (b) high magnification SEM images of NiCo-precursor/$Cu(OH)_2$/Cu.

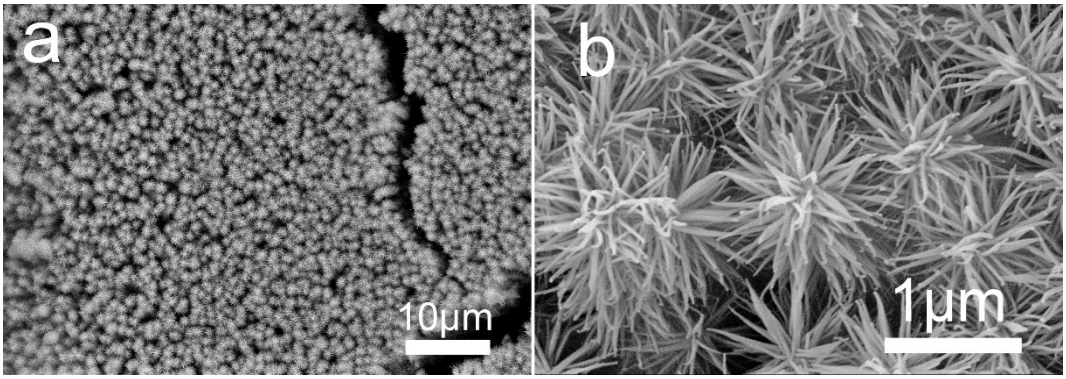


Fig. S6 (a) Low and (b) high magnification SEM images of $NiCo_2O_4/Cu_xO$/Cu.

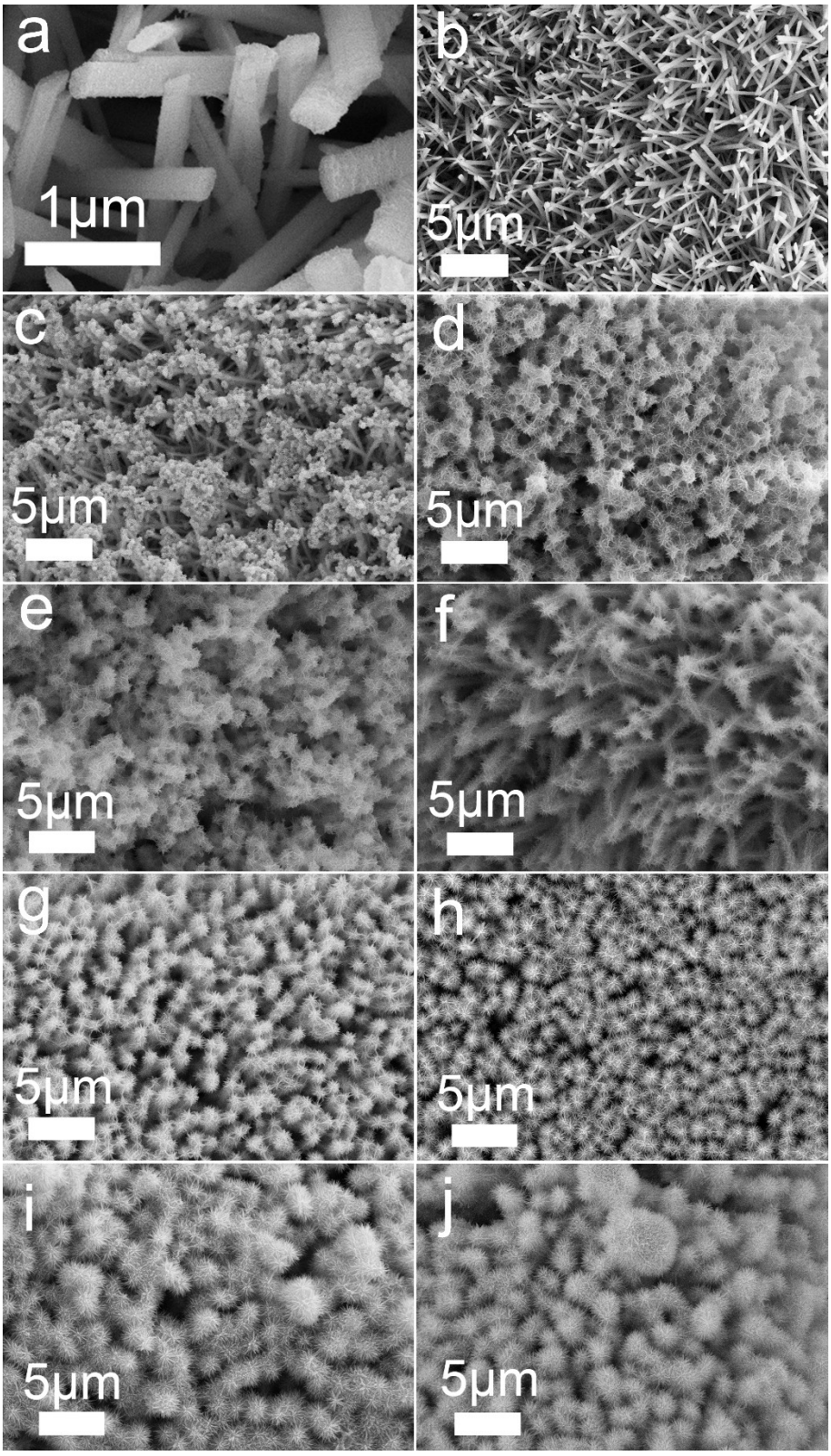


Fig. S7 SEM images of NiCo-precursor/$Cu(OH)_2$/Cu prepared with different hydrothermal reaction time: (a, b) 0.5 h, (c) 1 h, (d) 2 h, (e) 3 h, (f) 4 h, (g) 5 h, (h) 6 h, (i) 7 h, (j) 8 h.

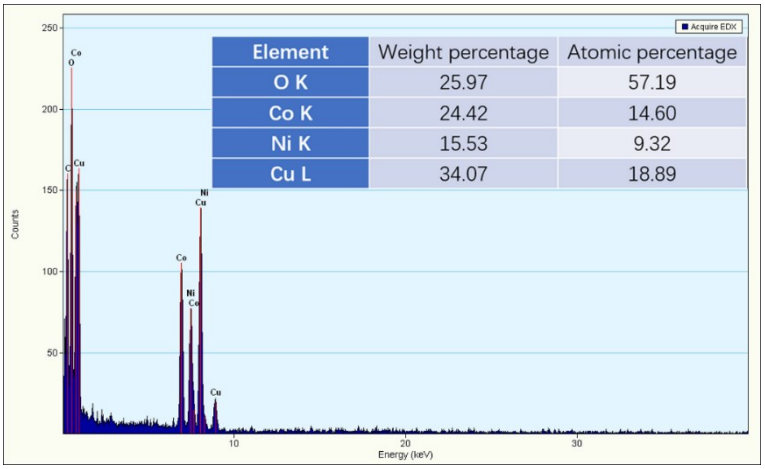


Fig. S8 EDS spectrum of $NiCo_2O_4/Cu_xO$. C is attributed to the carbon support film in the copper mesh.

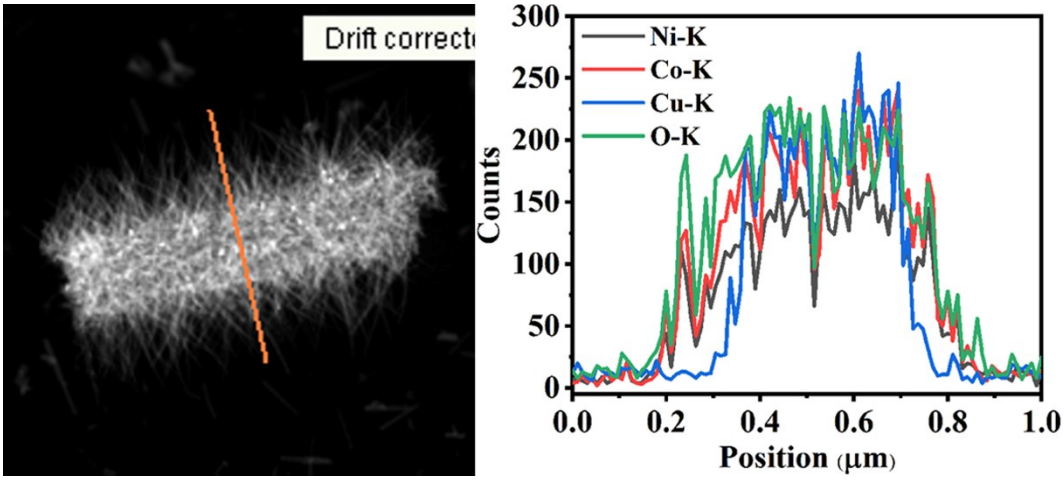


Fig. S9 HAADF images and the corresponding line-scan elemental distribution curves of $NiCo_2O_4/Cu_xO$.

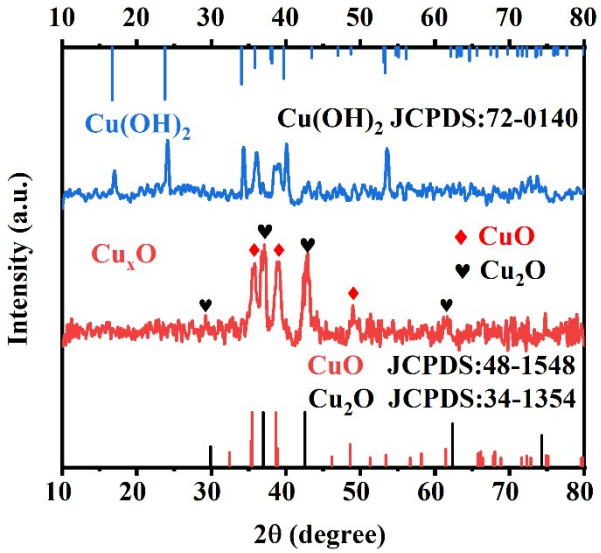


Fig. S10 The XRD patterns of the $Cu(OH)_2$ and $Cu_xO$ scraped off the substrate carefully.

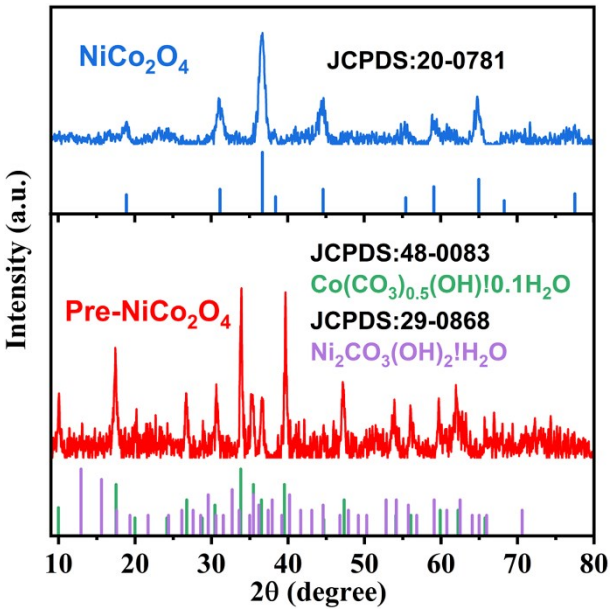


Fig. S11 The XRD patterns of the NiCo-precursor and $NiCo_2O_4$ scraped off the substrate carefully.

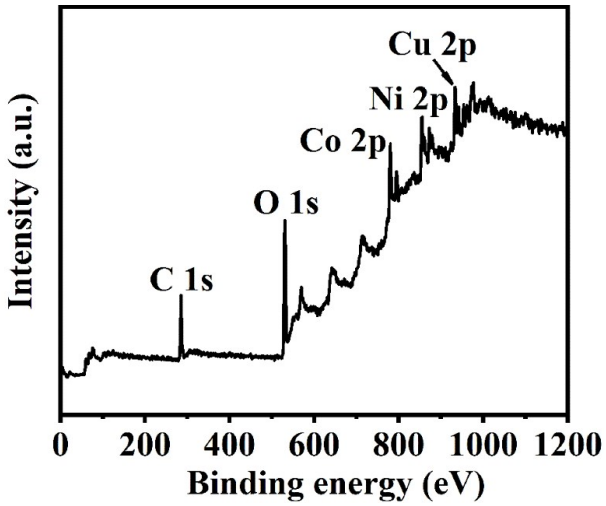


Fig. S12 Survey XPS spectra of $NiCo_2O_4/Cu_xO/Cu$.

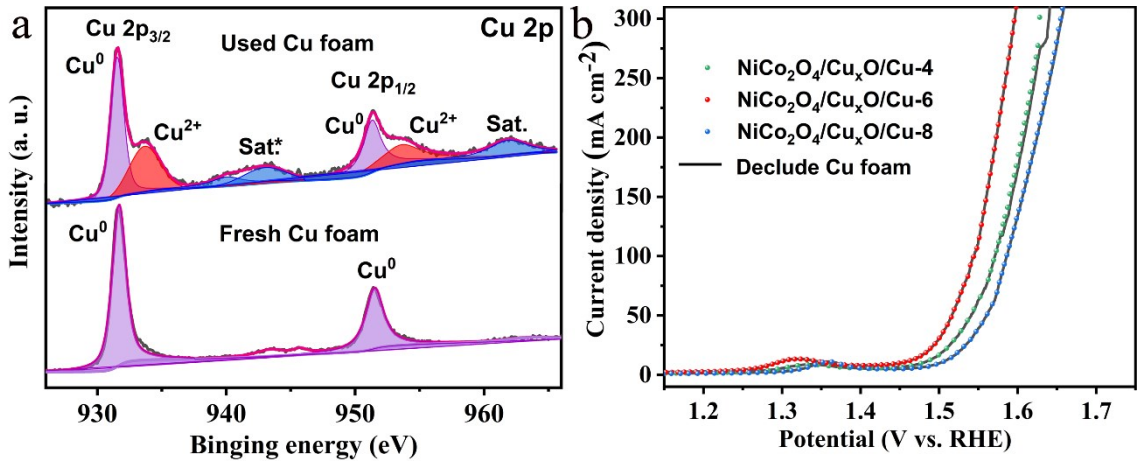


Fig. S13 (a) High-resolution XPS spectra of Cu 2p of Cu foam before and after i~t test (1.65 V vs. RHE) for 1 h. (b) LSV curves of $NiCo_2O_4/Cu_xO$/Cu-4/6/8 before and after deducting the current of Cu foam.

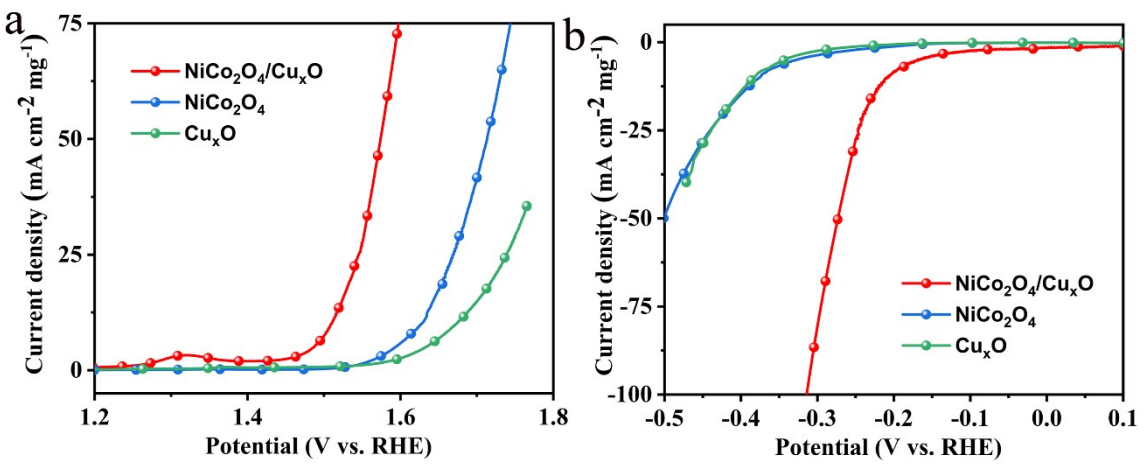


Fig. S14 The mass activity of the catalysts: (a) OER and (b) HER. The mass loadings are 4.10 mg $cm^{-2}$ for $NiCo_2O_4/Cu_xO/Cu$, 2.90 mg $cm^{-2}$ for $NiCo_2O_4/Cu$, and 3.57 mg $cm^{-2}$ for $Cu_xO/Cu$, respectively.

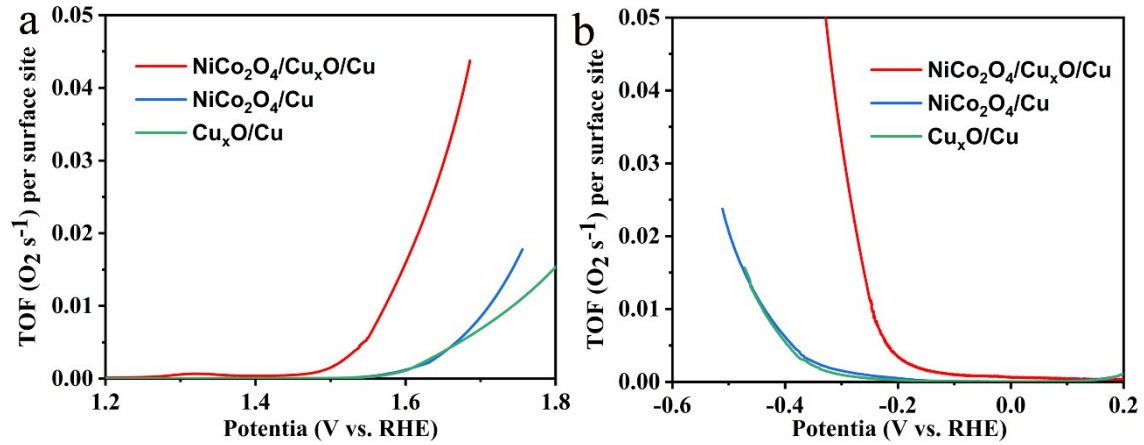


Fig. S15 The TOF of the catalysts: (a) OER and (b) HER. The TOF values are calculated by the following equation: TOF ($s^{-1}$) = ($|j| \times A$) / ($n \times F \times m$). $j$ (A $cm^{-2}$) is the current density. A is the geometric surface area of the electrode (1 $cm^2$). n is the number of electrons transferred in the reaction (n = 4 in OER and n = 2 in HER). F is the Faraday constant (96500 C $mol^{-1}$). m (mol) is the mole number of transition metals loaded on the Cu foam. It should be noted that the mass loading includes the Cu substrate oxidized during calcination, which has no special morphology and is mostly covered by the nanotrees, and all transition metals atoms are regarded as active sites (including Ni, Co, and Cu), making the real TOF underestimated seriously. The molar ratio of $NiCo_2O_4$ to $Cu_xO$ in $NiCo_2O_4/Cu_xO/Cu$ is determined by ICP results (Table S2). The molar ratio of $Cu_2O$ to CuO in $Cu_xO$ is determined by XPS results (Table S3).

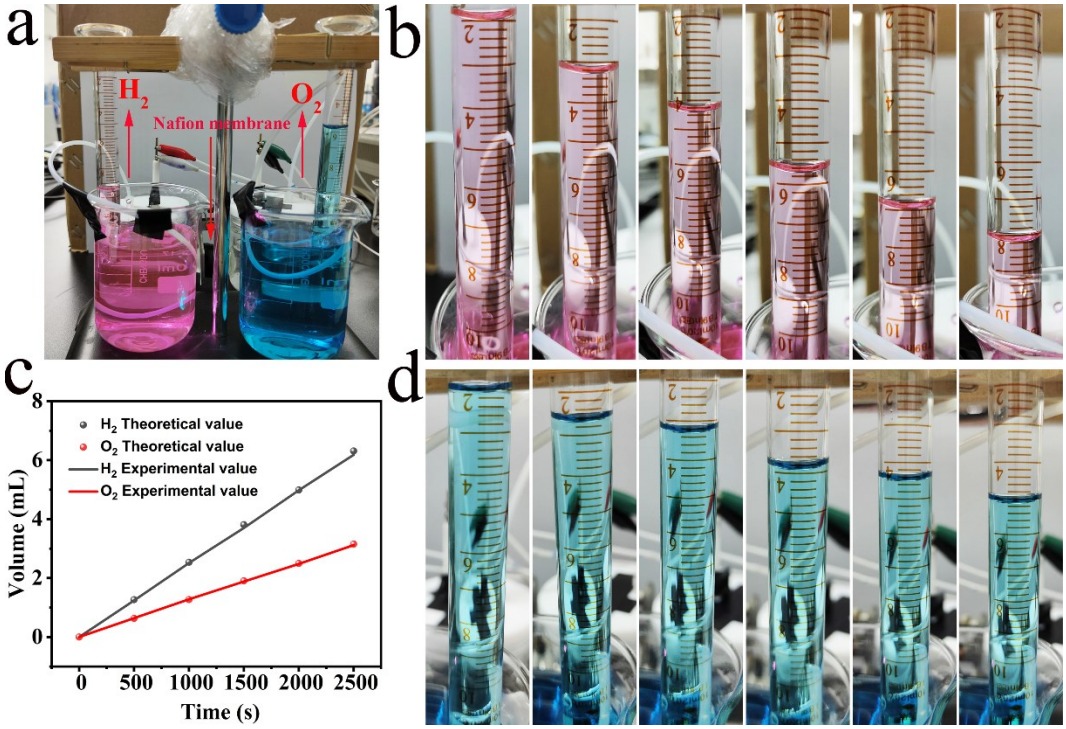


Fig. S16 Faradaic efficiency evaluated by the drainage method: (a) Device of drainage method. (b) $H_2$ and (d) $O_2$ collected at 0, 500, 1000, 1500, 2000, 2500 s. (c) The volume of $H_2$ and $O_2$ as a function of time.

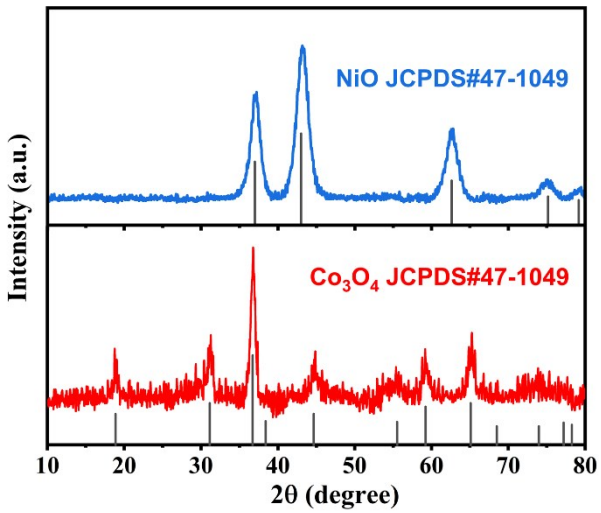


Fig. S17 The XRD patterns of $Co_xO_y$ and $Ni_xO_y$.

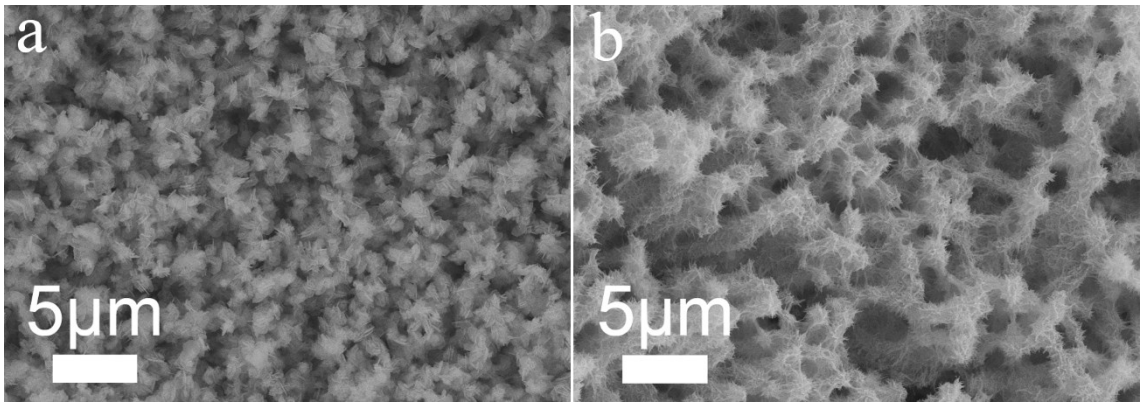


Fig. S18. The SEM images of (a) $Co_xO_y/Cu_xO/Cu$ and (b) $Ni_xO_y/Cu_xO/Cu$.

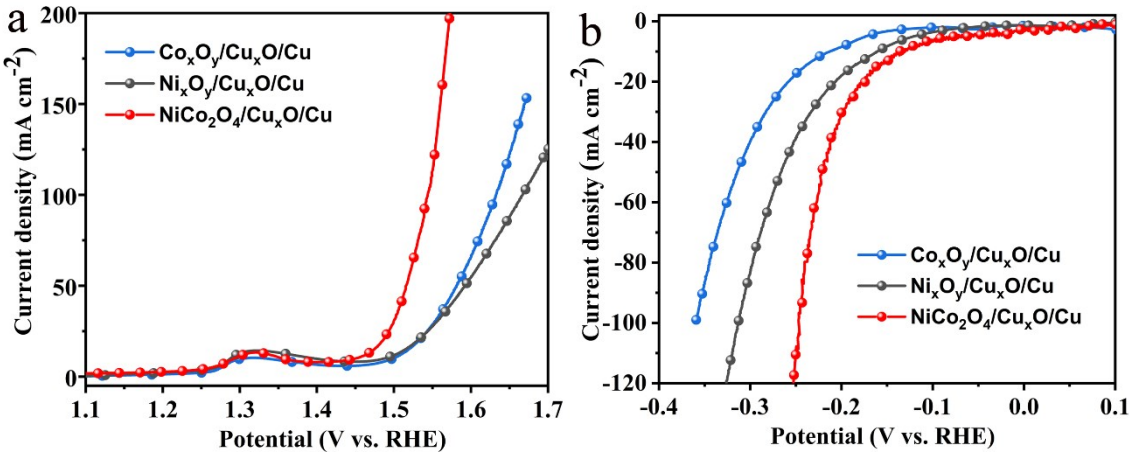


Fig. S19. LSV curves of (a) OER and (b) HER for $NiCo_2O_4/Cu_xO/Cu$, $Co_xO_y/Cu_xO/Cu$, and $Ni_xO_y/Cu_xO/Cu$.

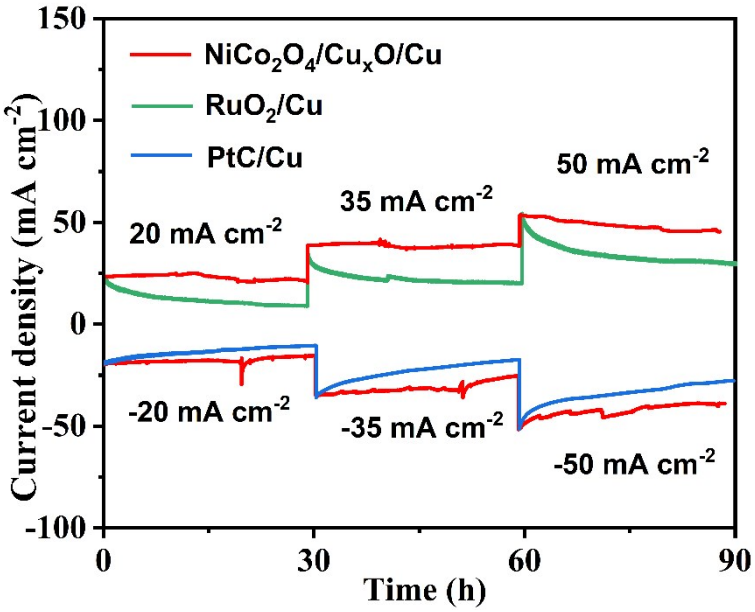


Fig. S20 Multipotentiometry measurement for catalysts in KOH (1 M) solution. The two current fluctuations of $NiCo_2O_4/Cu_xO/Cu$ in HER (~20 h and ~51 h) are caused by the replenishment of the internal filling solution of the reference electrode.

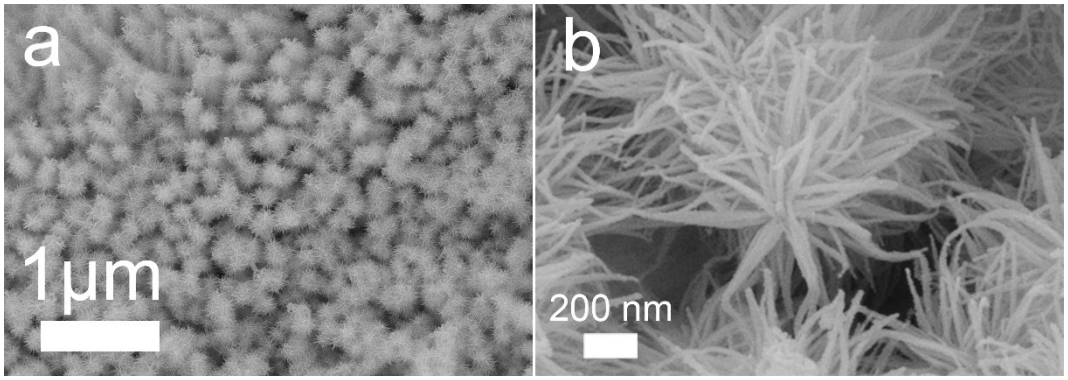


Fig. S21 (a) Low and (b) high magnification SEM images of $NiCo_2O_4/Cu_xO/Cu$ after overall water splitting reaction in KOH (1 M) solution for 30 h.

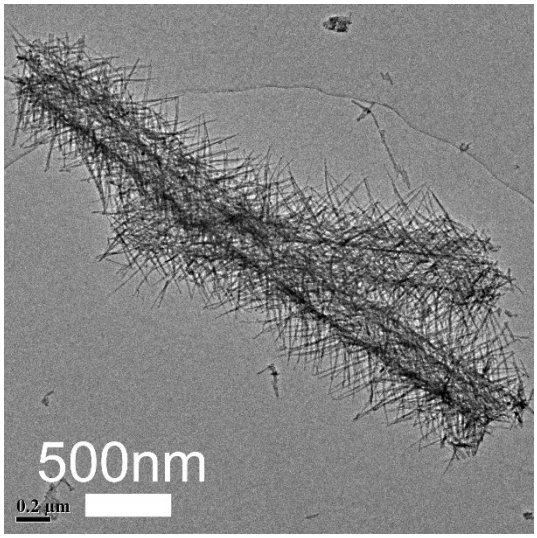


Fig. S22 TEM image of $NiCo_2O_4/Cu_xO$ after overall water splitting reaction in KOH (1 M) solution for 30 h.

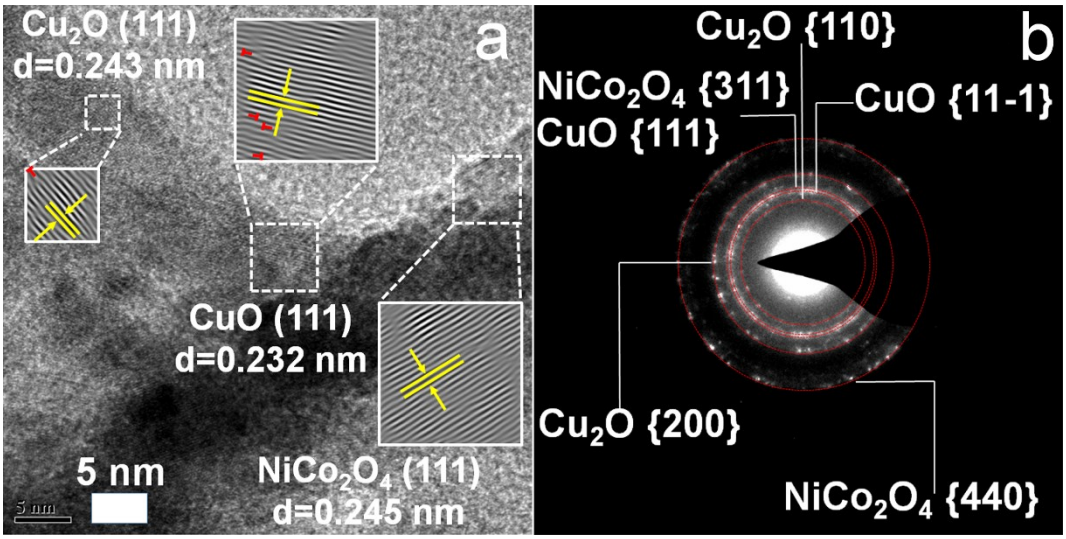


Fig. S23 (a) HRTEM image and (b) SAED pattern of $NiCo_2O_4/Cu_xO/Cu$ after overall water splitting reaction in KOH (1 M) solution for 30 h.

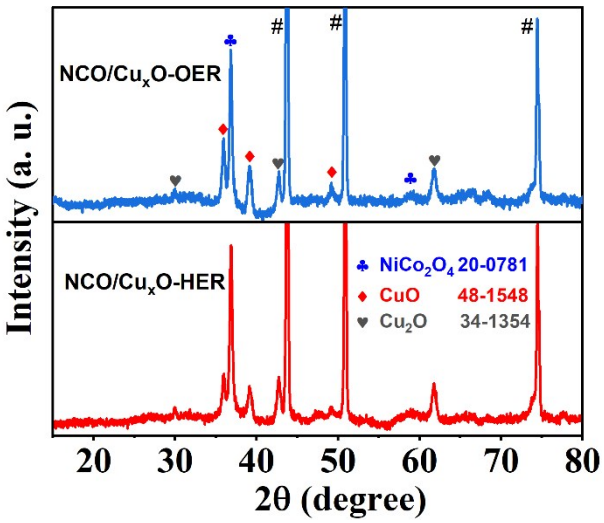


Fig. S24 XRD patterns of $NiCo_2O_4/Cu_xO/Cu$ after HER for 150 h and OER for 125 h in KOH (1 M) solution.

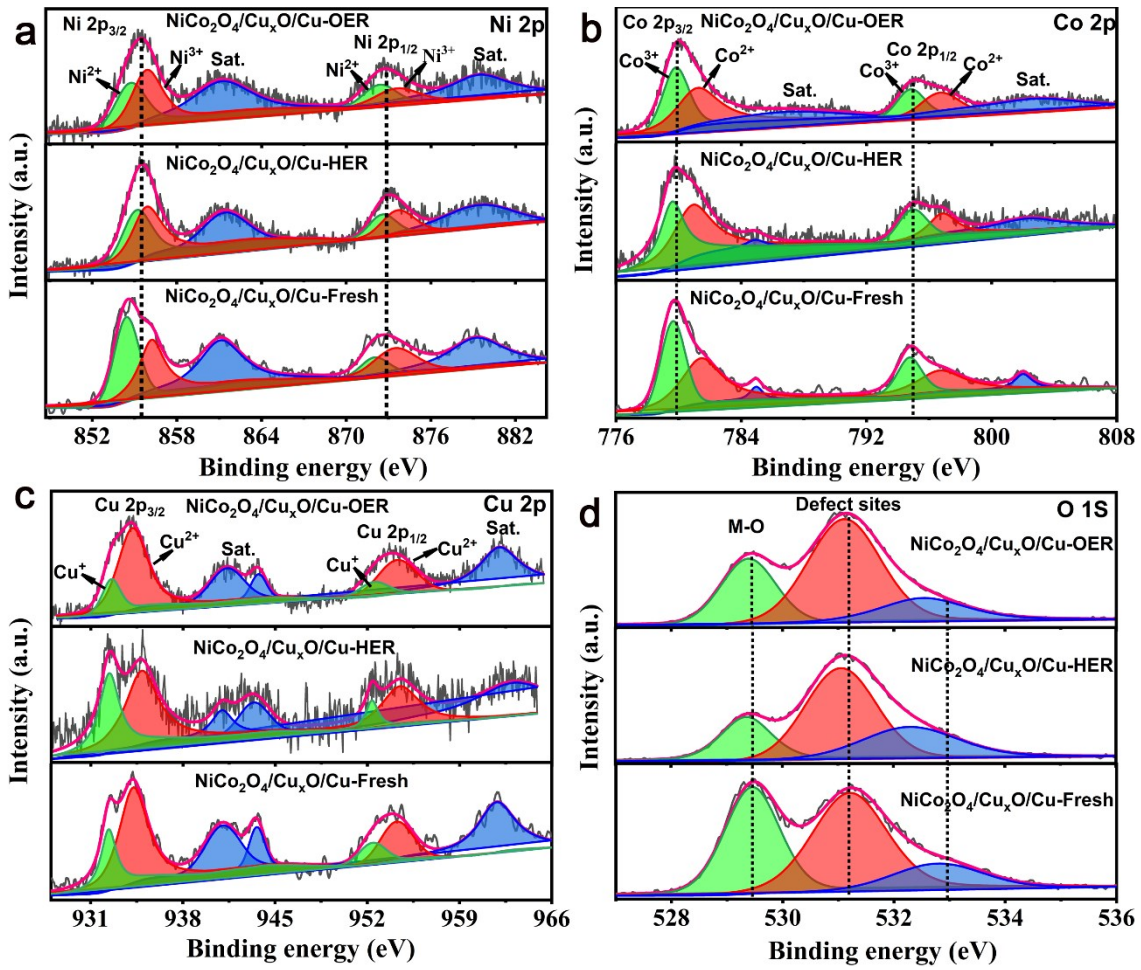


Fig. S25 High-resolution XPS spectra of (a) Ni 2p, (b) Co 2p, (c) Cu 2p, and (d) O 1s of $NiCo_2O_4/Cu_xO/Cu$ after HER for 150 h and OER for 125 h in KOH (1 M) solution.

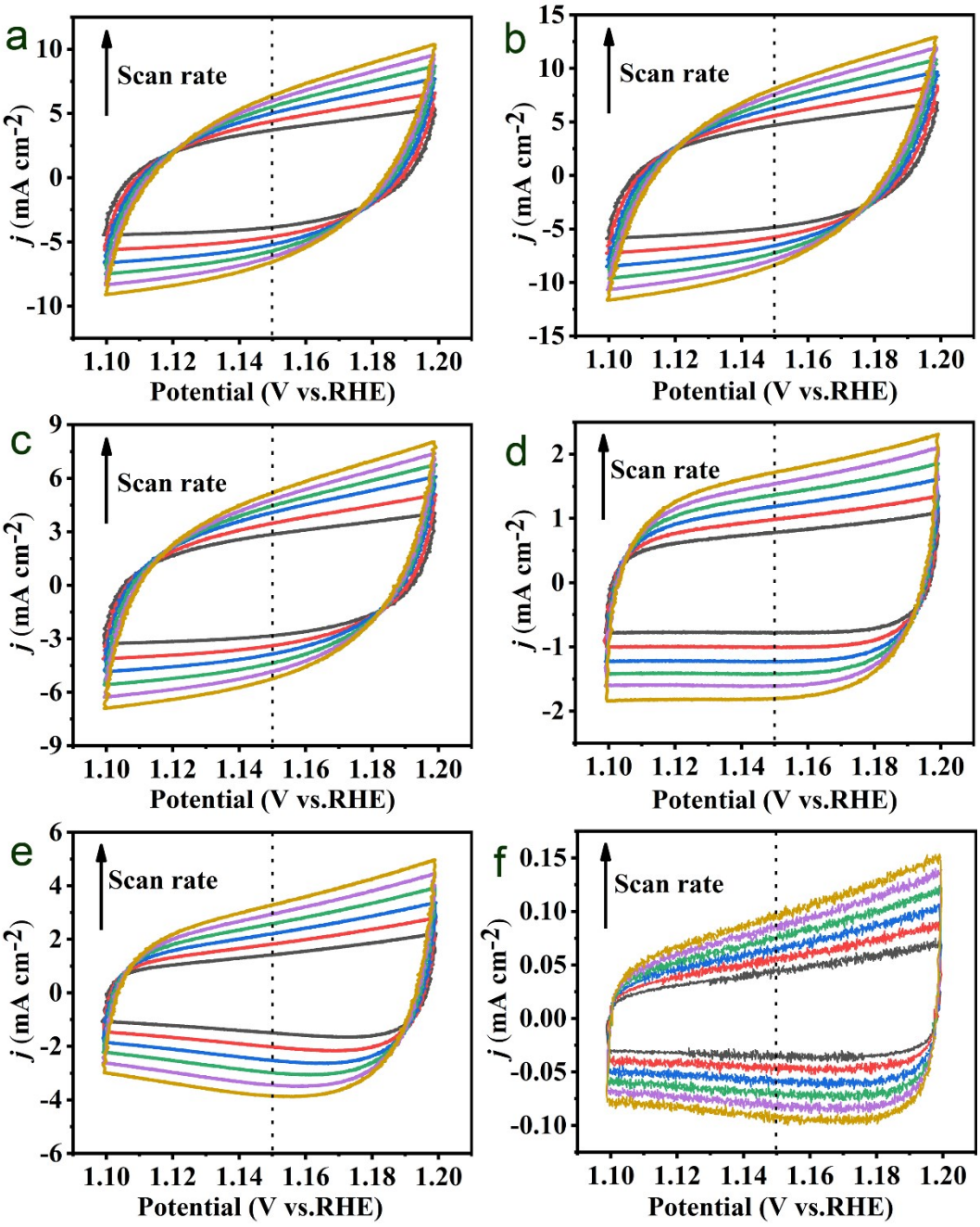


Fig. S26 CV curves of (a) $NiCo_2O_4/Cu_xO/Cu$-4, (b) $NiCo_2O_4/Cu_xO/Cu$-6, (c) $NiCo_2O_4/Cu_xO/Cu$-8, (d) $NiCo_2O_4/Cu$, (e) $Cu_xO/Cu$, and (f) bare Cu foam with different scan rates (15, 20, 25, 30, 35, 40 mV $s^{-1}$) from 1.10 V to 1.20 V (vs. RHE).

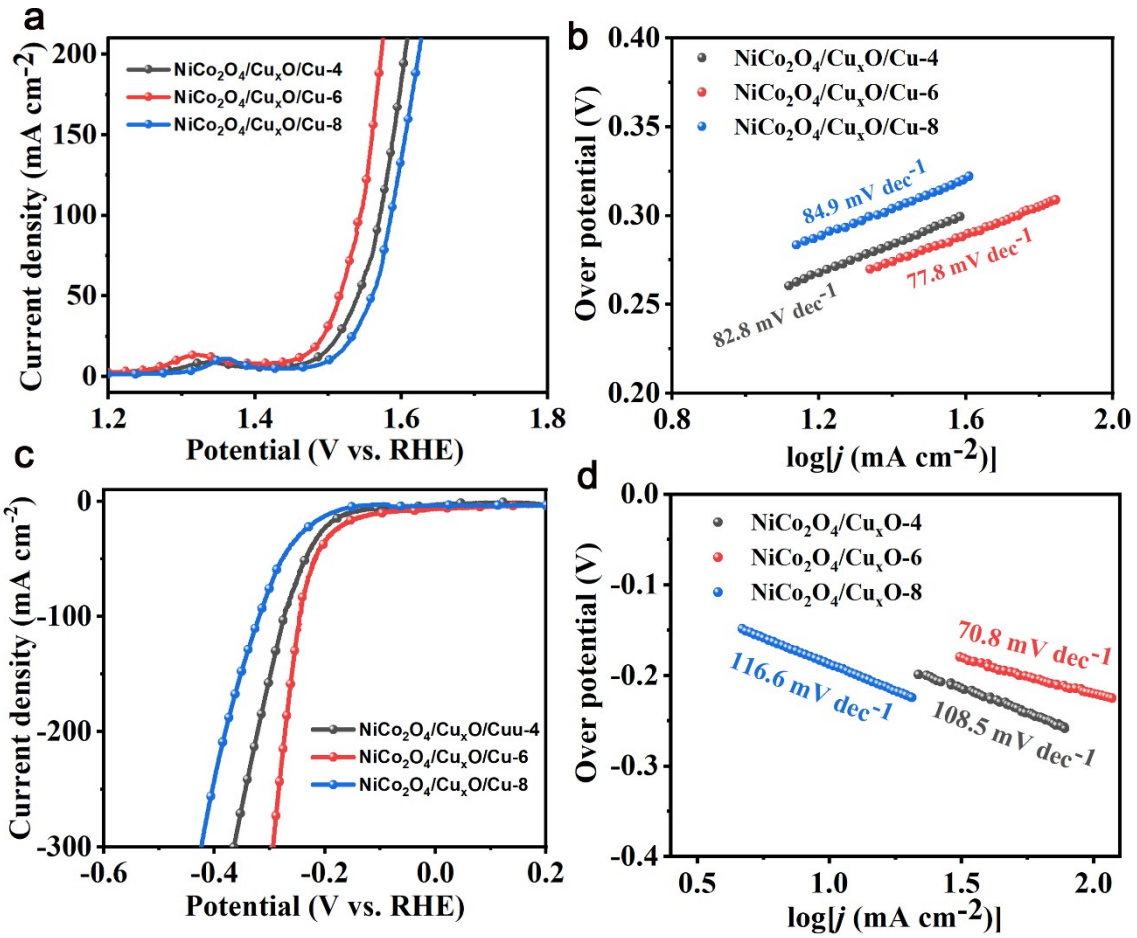


Fig. S27 (a) Polarization curves and (b) corresponding Tafel curves of $NiCo_2O_4/Cu_xO$/Cu-4/6/8 for OER. (c) Polarization curves and (d) corresponding Tafel curves of $NiCo_2O_4/Cu_xO$/Cu-4/6/8 for HER.

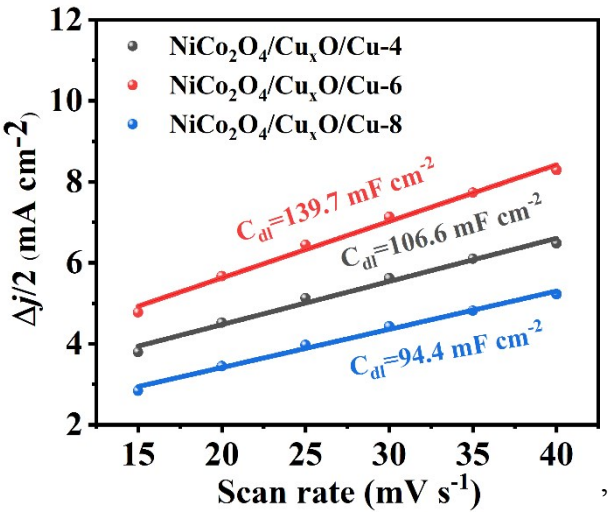


Fig. S28 Half of the capacitive current density ($\Delta j/2$) at 1.15 V (vs. RHE) plotted against different scan rates.

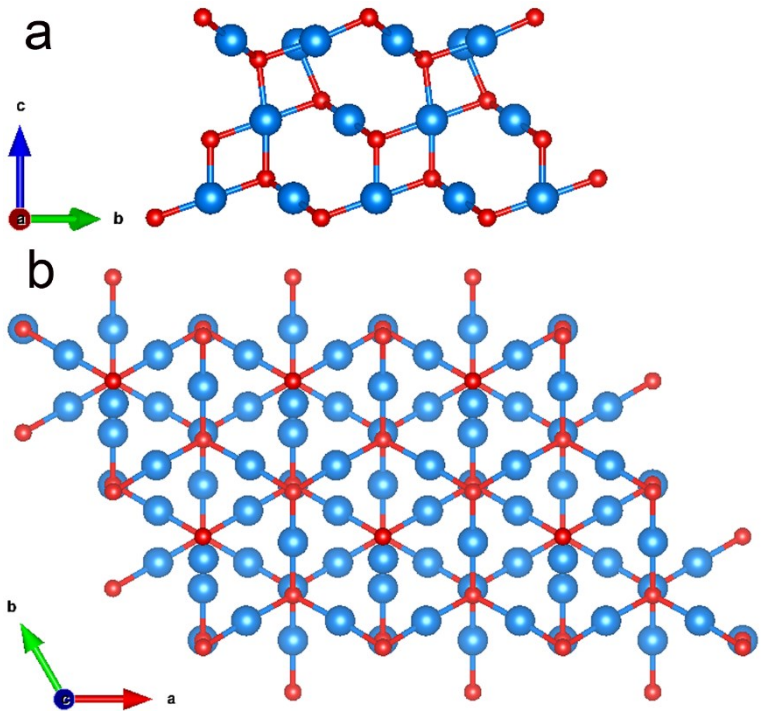


Fig. S29 DFT-optimized structure of $Cu_2O$ (111) in (a) the main view and (b) top view.

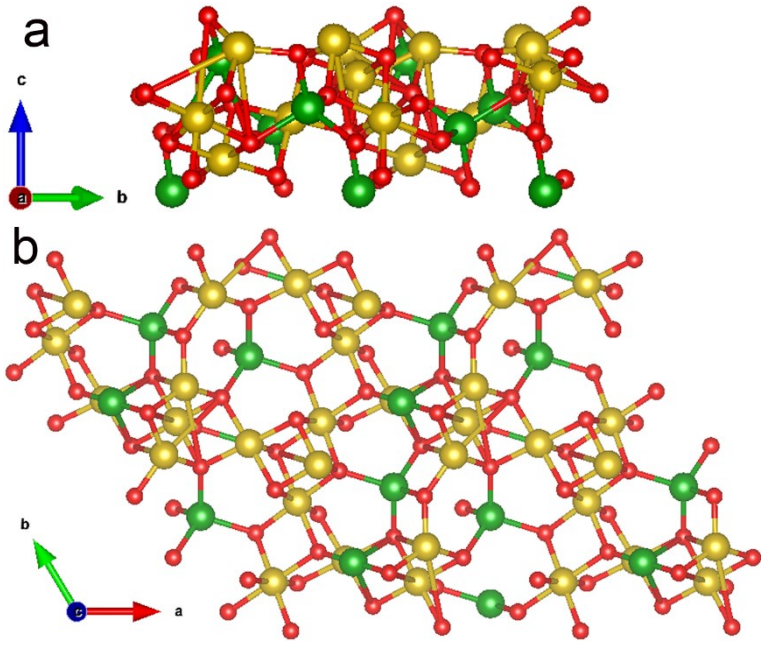


Fig. S30 DFT-optimized structure of $NiCo_2O_4$ (311) in (a) the main view and (b) top view.

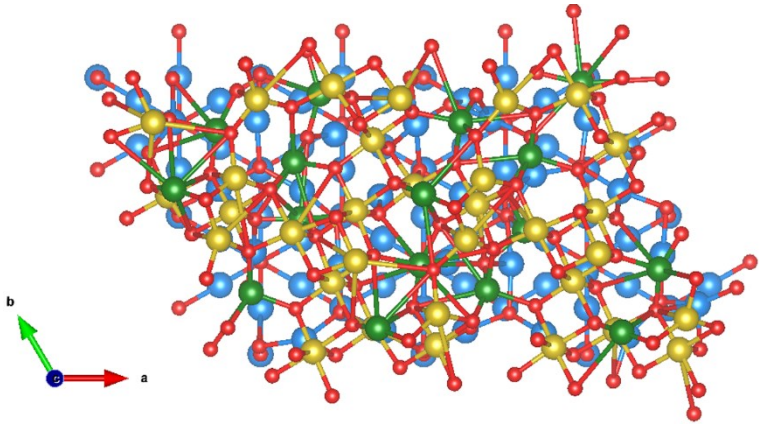


Fig. S31 DFT-optimized structure of $NiCo_2O_4(311)/Cu_2O$ (111) in top view.

Table S1 BET surface area of catalysts.

| Catalysts | $S_{BET}$ ($m^2$ $g^{-1}$) |
|---|---|
| $NiCo_2O_4/Cu_xO/Cu$-4 | 26.4225 |
| $NiCo_2O_4/Cu_xO/Cu$-6 | 28.3969 |
| $NiCo_2O_4/Cu_xO/Cu$-8 | 30.2371 |
| $NiCo_2O_4/Cu$ | 20.7776 |
| $Cu_xO/Cu$ | 20.3029 |
| Cu foam | 12.3401 |

Table S2 Element content of samples measured by ICP-OES.

| Sample | Measured element content in the diluted solution (mg $L^{-1}$) | | | Measured element content in the diluted solution (mmol $L^{-1}$) | | |
|---|---|---|---|---|---|---|
| | Co | Ni | Cu | Co | Ni | Cu |
| Pre-$NiCo_2O_4$ | 4.9230 | 2.4071 | -- | 0.0835 | 0.0410 | -- |
| $NiCo_2O_4$ | 3.2820 | 1.5963 | -- | 0.0557 | 0.0272 | -- |
| $NiCo_2O_4/Cu_xO$ | 1.9306 | 0.988 | 3.632 | 0.0327 | 0.0168 | 0.0567 |

*The diluted solution is made by dissolving the solid sample in an acid solution and diluting to a concentration range of 1-10 ppm.

Table S3 XPS peak area ratio of elements with different valence states.

| atom% | Ni | | Co | | Cu | | O | | |
|---|---|---|---|---|---|---|---|---|---|
| | $Ni^{3+}$ | $Ni^{2+}$ | $Co^{3+}$ | $Co^{2+}$ | $Cu^{2+}$ | $Cu^{+}$ | M-O | $O_u$ | $H_2O$ |
| $Cu_xO$ | - | - | - | - | 46.12 | 53.88 | 34.35 | 40.38 | 25.27 |
| $NiCo_2O_4$ | 50.91 | 49.09 | 49.95 | 50.05 | - | - | 38.52 | 40.93 | 20.55 |
| $NiCo_2O_4/Cu_xO$ | 55.22 | 44.78 | 43.27 | 56.73 | 70.52 | 29.48 | 39.48 | 47.80 | 12.72 |

Table S4 The etching rate of Cu.

| Sample | The total amount of Cu etched (mg) | | | | | |
|---|---|---|---|---|---|---|
| | 6 h | 12 h | 24 h | 30 h | 36 h | 48 h |
| $NiCo_2O_4/Cu_xO$ | 0.0745 | 0.1081 | 0.1241 | 0.1285 | 0.1327 | 0.1340 |
| Bare Cu foam | 0.9446 | 1.2936 | 1.8534 | 2.0541 | 2.2207 | 2.4631 |

*The geometric area of the working electrode is 1 $cm^2$ and the current density maintains at 10 mA $cm^{-2}$ for the OER. The total amount of Cu etched in alkaline solution is quantified by ICP-OES, including Cu ions in the electrolyte and $Cu^0$ deposited on the counter electrode.

Table S5 Comparison of OER electrocatalytic properties with other non-noble catalysts.

| Catalyst | Current density (mA $cm^{-2}$) | Overpotential vs. RHE (mV) | Electrolyte | Tafel slope (mV $dec^{-1}$) | Reference |
|---|---|---|---|---|---|
| $NiCo_2O_4/Cu_xO/Cu$ | 10<br>20<br>50 | 218<br>256<br>285 | 1.0 M KOH | 77.8 | This work |
| Cu/CuO/ Cu(OH)2 film | 10 | 580 | 1.0 M $Na_2CO_3$ | 90 | *Angew. Chem. Int. Ed.*, 2015, **54**, 2073 |
| $NiCo_2O_4$/Ni | 10 | 290 | 1.0 M NaOH | 53 | *Angew. Chem. Int. Ed.*, 2016, **55**, 6290 |
| $NiCo_2O_4$/Ni | 10 | 350 | 1.0 M KOH | 59.2 | *J. Catal.*, 2018, **357**, 238 |
| Cu-$Cu_2O$/CuO | 10 | 290 | 1.0 M KOH | 64 | *Angew. Chem., Int. Ed*. 2017, **56**, 4792 |
| $Cu_3P$/CuO | 10 | 315 | 1.0 M KOH | 74.8 | *ChemElectroChem* 2018, **5**, 2064 |
| Reduced $NiCo_2O_4$ | 10 | 240 | 1.0 M KOH | 52 | *J. Am. Chem. Soc.*, 2018, **140**, 13644 |
| NiFeCuP@$Ni_3S_2$/NiF | 10 | 230 | 1.0 M KOH | 42 | *ACS. Appl. Mater. Interfaces*, 2020,**12**,36268-36276 |
| FeCoNi-$NiCo_2O_4$/CC | 50 | 302 | 1.0 M KOH | 71.5 | *ACS Appl. Mater. Interfaces*, 2017, **9**, 36917 |
| $Ni_3S_2/MnO_2$ | 10 | 260 | 1.0 M KOH | 61 | *Appl. Catal. B Environ*., 2019, **254**, 329-338 |
| $CoS_x$ | 10 | 375 | 1.0 M KOH | 77 | *J. Mater. Chem. A*, 2020, **8**, 7647-7652 |
| meso-Fe-$MoS_2/CoMo_2S_4$ | 10 | 290 | 1.0 M KOH | 65 | *ACS Nano*, 2020, **14**, 4141-4152 |
| Co-Se-S-O | 10 | 254 | 1.0 M KOH | 86.1 | *ACS Appl. Mater. Interfaces* 2018, **10**, 8231−8237 |
| $WO_3$-Vo | 10 | 590 | 0.5 M $H_2SO_4$ | 183.3 | *CCS Chem*., 2020, 2, 1553-1561 |
| NiCo LDH nanosheets | 10 | 367 | 1 M KOH | 40 | *Nano Lett.*, 2015, 15, 1421−1427 |
| NiCoP/NF | 10 | 280 | 1 M KOH | 87 | *Nano Lett*., 2016, 16, 7718−7725 |

Table S6 Comparison of HER electrocatalytic properties with other non-noble catalysts.

| Catalyst | Current density (mA $cm^{-2}$) | Overpotential vs. RHE (mV) | Electrolyte | Tafel slope (mV $dec^{-1}$) | Reference |
|---|---|---|---|---|---|
| $NiCo_2O_4/Cu_xO/Cu$ | 10<br>20<br>50 | 92<br>165<br>215 | 1.0 M KOH | 70.8 | This work |
| VOOH/Ni | 10 | 164 | 1.0 M KOH | 104 | *Angew. Chem. Int. Ed.*, 2017, **56**, 573 |
| $NiCo_2O_4$/Ni | 10 | 110 | 1.0 M NaOH | 49.7 | *Angew. Chem. Int. Ed.*, 2016, **55**, 6290 |
| $NiCo_2O_4$/Ni | 10 | 200 | 1.0 M KOH | 71.2 | *J. Catal.*, 2018, **357**, 238 |
| $Ni_3S_2/MnO_2$ | 10 | 102 | 1.0 M KOH | 69 | *Appl. Catal. B Environ.*, 2019, **254**, 329-338 |
| meso-Fe-$MoS_2/CoMo_2S_4$ | 10 | 122 | 1.0 M KOH | 90 | *ACS Nano*, 2020, 14, 4141-4152 |
| Reduced $NiCo_2O_4$ | 10 | 135 | 1.0 M KOH | 52 | *J. Am. Chem. Soc.*, 2018, **140**, 13644 |
| FeCoNi-$NiCo_2O_4$/CC | 20 | 151 | 1.0 M KOH | 114.2 | *ACS Appl. Mater. Interfaces*, 2017, **9**, 36917 |
| Cu@$Cu_2S$@$NiCoO_{2-x}S_x$ | 20 | 203 | 1.0 M KOH | 63 | *J. Mater. Chem. A*, 2020, **8**, 14746 |
| (Ni, Fe)$S_2$@$MoS_2$ | 10 | 130 | 1.0 M KOH | 101.2 | *Appl. Catal. B Environ.*, 2019, **247**, 109 |
| $Co_3O_4/MoS_2$ | 10 | 205 | 1.0 M KOH | 98 | *Appl. Catal. B Environ.*, 2019, **248**, 202 |
| NiCoP/NF | 10 | 32 | 1.0 M KOH | 37 | *Nano Lett*., 2016, 16, 7718−7725 |

Table S7 Comparison of overall water splitting electrocatalytic properties with other non-noble catalysts.

| Catalyst | Current density (mA $cm^{-2}$) | Potential (V) | Electrolyte | Reference |
|---|---|---|---|---|
| $NiCo_2O_4/Cu_xO/Cu$ | 10 | 1.61 | 1.0 M KOH | This work |
| VOOH/Ni | 10 | 1.61 | 1.0 M KOH | *Angew. Chem. Int. Ed.*, 2017, **56**, 573 |
| Ni-Fe-O | 10 | 1.64 | 1.0 M KOH | *Adv. Energy Mater.*, 2018, **8**, 1701347 |
| $NiCo_2O_4$/Ni | 10 | 1.65 | 1.0 M NaOH | *Angew. Chem. Int. Ed.*, 2016, **55**, 6290 |
| $NiCo_2O_4$/Ni | 10 | 1.61 | 1.0 M KOH | *J. Mater. Chem. A*, 2018, **6**, 20076 |
| CoP/N-CNT | 10 | 1.64 | 1.0 M KOH | *J. Am. Chem. Soc*. 2018, **140**, 2610–2618 |
| meso-Fe-$MoS_2/CoMo_2S_4$ | 10 | 1.62 | 1.0 M KOH | *ACS Nano*, 2020, **14**, 4141-4152 |
| Reduced $NiCo_2O_4$ | 10 | 1.61 | 1.0 M KOH | *J. Am. Chem. Soc.*, 2018, **140**, 13644 |
| FeCoNi-$NiCo_2O_4$/CC | 50 | 1.65 | 1.0 M KOH | *ACS Appl. Mater. Interfaces*, 2017, **9**, 36917 |
| $Cu_{2.75}Fe_{0.25}P$ | 100 | 1.85 | 1.0 M KOH | *Nanoscale*, 2020, **12**, 17769-17779 |
| (Ni, Fe)$S_2$@$MoS_2$ | 10 | 1.56 | 1.0 M KOH | *Appl. Catal. B*, 2019, **247**, 109 |
| NiFe-Oxide/CC | 10 | 1.67 | 1.0 M KOH | *ACS Appl. Mater. Interfaces*, 2017, **9**, 41906 |
| S-$NiFe_2O_4$/Ni | 10 | 1.65 | 1.0 M KOH | *Nano Energy*, 2017, **40**, 264 |
| NiCoP/NF | 10 | 1.58 | 1.0 M KOH | *Nano Lett*., 2016, 16, 7718−7725 |

Table S8 XPS peak area ratio of elements with different valence states of $NiCo_2O_4/Cu_xO/Cu$ before and after long-term stability tests.

| Atom% | Ni | | Co | | Cu | | O | | |
|---|---|---|---|---|---|---|---|---|---|
| | $Ni^{3+}$ | $Ni^{2+}$ | $Co^{3+}$ | $Co^{2+}$ | $Cu^{2+}$ | $Cu^{+}$ | M-O | $O_u$ | $H_2O$ |
| Fresh | 55.22 | 44.28 | 43.27 | 56.73 | 70.52 | 29.48 | 39.48 | 47.80 | 12.72 |
| After HER | 55.62 | 44.38 | 45.36 | 54.64 | 65.64 | 34.36 | 21.97 | 52.46 | 25.57 |
| After OER | 55.42 | 44.58 | 45.86 | 54.14 | 77.72 | 22.28 | 27.57 | 56.12 | 16.31 |

Table S9 Bader charges analysis.

| Samples | Element | Number of atoms | Number of valence electrons in an atom | Total number of valence electrons | Total number of valence electrons in optimized configuration | Total number of valence electrons transferred |
|---|---|---|---|---|---|---|
| $Cu_2O$ | Cu | 72 | 11 | 792 | 750.84713 | - |
| | O | 36 | 6 | 216 | 257.15290 | - |
| | $Cu_2O$ | 108 | - | 1008 | 1008.00007 | - |
| $NiCo_2O_4$ | Co | 32 | 9 | 288 | 245.80387 | - |
| | Ni | 16 | 10 | 160 | 144.23292 | - |
| | O | 64 | 6 | 384 | 441.96326 | - |
| | $NiCo_2O_4$ | 112 | - | 832 | 832.00005 | - |
| $NiCo_2O_4/Cu_2O$ | Co | 32 | 9 | 288 | 246.11820 | 0.31433 |
| | Ni | 16 | 10 | 160 | 143.91724 | -0.31568 |
| | O-$NiCo_2O_4$ | 64 | 6 | 384 | 447.48381 | 5.52055 |
| | Cu | 72 | 11 | 792 | 745.49570 | -5.35143 |
| | O-$Cu_2O$ | 36 | 6 | 216 | 256.98512 | -0.16778 |
| | $NiCo_2O_4/Cu_2O$ | 220 | - | 1840 | 1840.00007 | - |